Available online at www.sciencedirect.com
ScienceDirect
Journal of Power Sources 160 (2006) 1170–1182
JOURNAL OF POWER SOURCES
www.elsevier.com/locate/jpowsour

Dynamic modeling of proton exchange membrane fuel cell using non-integer derivatives

M. Usman Iftikhar [a], D. Riu [a,*], F. Druart [b], S. Rosini [b], Y. Bultel [b], N. Retière [a]

[a] *Laboratoire d'Electrotechnique de Grenoble (LEG), UMR 5529 CNRS-INPG-UJF, ENSIEG, BP 46, 38402 Saint Martin d'Hères, France*
[b] *Laboratoire d'Electrochimie et de Physico-Chimie des Matériaux et des Interfaces (LEPMI), UMR 5631 CNRS-INPG-UJF, ENSEEG, BP 75, 38402 Saint Martin d'Hères, France*

Received 8 November 2005; received in revised form 21 February 2006; accepted 9 March 2006
Available online 11 May 2006

Abstract

The modeling of proton exchange membrane fuel cells (PEMFC) may work as a powerful tool in the development and widespread testing of alternative energy sources in the next decade. In order to obtain a suitable PEMFC model, which can be used in the analysis of fuel cell-based power generation systems, it is necessary to define the values of a specific group of modeling parameters. In this paper, the authors propose a dynamic model of PEMFC, the originality of which lays on the use of non-integer derivatives to model diffusion phenomena. This model has the advantage of having least number of parameters while being valid on a wide frequency range and allows simulating an accurate dynamic response of the PEMFC.

In this model, the fuel cell is represented by an equivalent circuit, whose components are identified with the experimental technique of electrochemical impedance spectroscopy (EIS). This identification process is applied to a commercially available air-breathing PEMFC and its relevance is validated by comparing model simulations and laboratory experiments. Finally, the dynamic response derived from this fractional model is studied and validated experimentally.

Keywords: Proton exchange membrane fuel cell (PEMFC); Fractional modeling; Electrochemical impedance spectroscopy (EIS); Dynamic response; Equivalent circuits

1. Introduction

It is believed that there will be a time in the future when global energy demands will be met by some sources of energy other than fossil fuels. Thus, fuel cells, in particular proton exchange membrane fuel cells (PEMFC), are expected to play a major role in the future energy sector. PEMFC are particularly attractive for use in vehicles as a replacement to the internal combustion engines. They also seem to be a promising source to be used in residences, industries and small- and large-scale distributed generation systems. The low operating temperature of a PEMFC (typically <90 °C) allows easy start-up and fast response to load variations and operating conditions. Nevertheless, several issues need to be resolved before fuel cells can be commercially viable. Indeed, the need of precise water management, the dehydration of membrane, the complex electrode kinetics, the mass transport and the slow rate of oxygen reduction are the most significant limiting factors on the fuel cell performances.

In order to better understand the physical phenomena in the fuel cells and describe their steady state and dynamic behaviors, the modeling of fuel cells has become more and more important over the years in order to simulate the behaviour of the fuel cell integrated in a power system. Such model must be sufficiently complex to take into account all the electrochemical phenomena and, at the same time, should be able to be integrated into a complete system simulation. Furthermore, these models must be modular so as to allow easily the testing of various technological solutions.

In this article, the authors have focused on the dynamic modeling of a fuel cell. Such modeling to simulate the transient response of a PEMFC is studied only recently. In the past, the

* Corresponding author. Tel.: +33 4 76 82 62 83; fax: +33 4 76 82 63 00.
E-mail addresses: usmanabc@yahoo.com (M.U. Iftikhar), Delphine.Riu@leg.ensieg.inpg.fr (D. Riu).

0378-7753/$ – see front matter © 2006 Elsevier B.V. All rights reserved.
doi:10.1016/j.jpowsour.2006.03.044

Nomenclature

Nomenclature

b	Tafel slope (V dec^{-1})
C_{dl}	double layer capacitance (F m^{-2})
C	concentration of species (mol m^{-3})
D	diffusion coefficient (m^2 s^{-1})
E	potential (V)
F	Faraday's constant (96,500 C mol^{-1})
j	current density (A m^{-2})
j_0	exchange current density (A m^{-2})
j_l	limiting current density (A m^{-2})
n_e	total number of exchanged electrons
P	anode and cathode gas pressure (Pa)
R	ideal gas constant (8.314 J mol^{-1} K^{-1})
R_m	membrane resistance (Ω m^2)
s	Laplace operator = $i \times \omega$
T	temperature (K)
U_{cell}	cell potential (V)
Z	impedance (Ω)

Greek symbols

δ	gas diffusion layer thickness (m)
ε	porosity
γ	roughness factor (m^2 m^{-2})
η	overpotential (V)
ω	angular frequency (rad s^{-1})
τ	time constant (s)

Subscripts and superscripts

a	anode
c	cathode
k	either anode or cathode
m	membrane
*	referring to the gas channel/gas diffusion layer interface
eff	referring to the effective (apparent) value

mathematical models of the PEMFC have usually been restricted to the steady state conditions. Bernardi [1] first proposed a one-dimensional model in order to study the water management and to identify the humidification conditions which induce either the dehydration of the membrane or excessive flooding. The sensitivity to the water balance of the PEMFC performance was demonstrated. Some other models were derived from the original one to take into account heat management [2], mass transport in the gas diffusion electrode [3] or to introduce a different treatment of the electrochemical reaction [4]. Bernardi et al. [5] and Springer et al. [6] also presented a one-dimensional model to investigate the factors that limit cell performance and to elucidate the mass transport mechanism within the complex network of gas, liquid and solid phases constituting the gas diffusion electrode. Contrary to the previous models, this latter one considered the molar changes along the gas channel. These approaches made it possible to evaluate the losses in the cathode gas backing and the catalyst layer.

So far efforts have been made to model the problem in three dimensions. A higher dimensionality makes it possible to describe the hydrodynamics and multi component transport inside the flow channel for reactant distribution. Multi component models were thus developed for cathode or for whole PEMFC, for both single-phase [7] and two phase flow [8]. These models showed that the gas distributor geometry has a significant effect on the diffusion of the reactants and products in determining the performance of the cell. Moreover, they confirmed that the performance of cathode is strongly influenced by the presence of liquid water and its removal rate, especially at high current density.

The dynamic study of a fuel cell appears to be of great interest to provide detailed understanding of mass and charge transport through the gas diffusion electrodes and is of extreme importance for the control strategy and system management in power generation systems, especially when there are power injections into the network. Thus a first equivalent circuit was proposed to simulate the impedance spectrum of a PEMFC [9]. This study showed that the impedance of a fuel cell is a powerful tool in order to characterize the intra-electrode processes occurring in gas diffusion electrodes.

Some dynamic models of PEMFC [10–13] have been developed based on the physical and chemical knowledge of the phenomena occurring inside the cell. These models are generally implemented in Simulink–Matlab environment. Results indicated that the transient response of the PEMFC to reach steady state is less than 10 s. An important effect of water management was exhibited too [12].

Some other models were developed in a more "System" approach [14]. These models are relatively simple which allow correctly simulating the behavior of the fuel cell inserted in an electrical network. The main disadvantage of these models is that they are far away from the physics of the fuel cell, i.e. their parameters are physically non-representative. In parallel, some other multi-scale models were elaborated [15] to predict the dynamic and steady state behaviors for the triple contact (base of the electrochemical reaction). These models made it possible to describe quantitatively the reactional mechanisms, the polarization curves and impedance spectra of the fuel cell.

In this work, the authors have linked these two approaches (components and systems) by using the fractional approach in order to obtain an adequate model of fuel cell impedance, which can be used in a system simulation. Non-integer derivation has already been used to correctly model the diffusion phenomenon of magnetic field in electrical machines [16] which is a physical phenomenon similar to one found in the electrochemical devices. The resulting models are precise, having less number of parameters and being valid on a wide frequency range. Moreover, parameters of such non-integer order models have a close link with the physical characteristics of the machines. This method is very useful for the optimal real-time control of PEMFC running on a load.

In this study, the authors have thus used non-integer derivatives to model the diffusion phenomenon of gases on electrodes. Then, this new modeling technique is compared with the classical one while taking into account the characteristic response

of the fuel cell (i.e. polarization curves and impedance spectra). In order to identify the model parameters, a complete set of experimental results was obtained for a commercially available air-breathing PEMFC using the technique of impedance spectroscopy. Finally, the dynamic response derived from this fractional model is studied and validated experimentally.

2. Modeling of fuel cell

2.1. Hypotheses

The air-breathing PEMFC system is considered as isothermal and isobaric. Both these approximations appear to be valid since these conditions are normally achieved in a small single-cell experimental investigation. The total pressure at the anode and cathode compartment and within the gas diffusion electrodes is considered as constant. Moreover, ionic ohmic drop in the active layer and the electronic ohmic drop in the current collectors can be neglected owing to the high electronic and ionic conductivities, and thus lead to the absence of voltage drop. It is also supposed that the gas permeation in the membrane is negligible.

2.2. Modeling in steady-state regime

The physical model used to obtain the following governing equations for steady state and transient responses of PEMFC is based on a previous d.c. and a.c. model [15]. Fig. 1 shows a schematic illustration of a self-breathing PEMFC that consists in a membrane sandwiched between two gas diffusion electrodes, this assembly being pressed between two current collectors and end plate. A simplified view of an electrode and the induced variation of the concentration of reactant gazes along the width of diffusion layer are also presented.

In Fig. 1, δ represents the diffusion layer thickness, $C_k^* = P_k/RT$ is the concentration of oxygen (O_2) or hydrogen (H_2) in the gas channels, C_k the concentration of hydrogen or oxygen at the active layer/diffusion layer interface and P_k the gas pressure.

Far from the equilibrium, the hydrogen oxidation and oxygen reduction are classically described by the laws of Tafel [15]:

$$j_a = j_{0a} \exp\left(\frac{2.3|\eta_a|}{b_a}\right) \frac{C_{H_2}}{C^*_{H_2}} \quad \text{and}$$

$$j_c = j_{0c} \exp\left(\frac{2.3|\eta_c|}{b_c}\right) \frac{C_{O_2}}{C^*_{O_2}} \tag{1}$$

where j_{0k} is the exchange current density, b_k the Tafel slope, $|\eta_k| = |E_k - E_{th_k}|$ the absolute value of the overpotential, R the ideal gas constant and T is the temperature. The subscript "k" represents either anode (a) or cathode (c).

It has been shown in [15] that the ratio of the concentration of the gas at the interface is closely linked to the current density as follows:

$$\frac{C_k}{C_k^*} = 1 - \frac{j_k}{j_{kl}} \tag{2}$$

Finally, the equations (1) are expressed using the limiting current densities and introducing the roughness factor of the electrodes:

$$j_a = \gamma_a\, j_{0a} \exp\left(\frac{2.3|\eta_a|}{b_a}\right)\left(1 - \frac{j_a}{j_{la}}\right) \quad \text{and}$$

$$j_c = \gamma_c\, j_{0c} \exp\left(\frac{2.3|\eta_c|}{b_c}\right)\left(1 - \frac{j_c}{j_{lc}}\right) \tag{3}$$

While the limiting current density can be defined as:

$$j_{lk} = \frac{D_k^{\text{eff}}}{\delta} C_k^* n_{e,k} F \tag{4}$$

where γ_k is the roughness factor, n_{ek} the number of exchanged electrons, F the Faraday's constant, $D_k^{\text{eff}} = \varepsilon^{1.5} D_k$ the effective gas diffusion coefficient and ε, the porosity of electrodes. The coefficient γ_k is introduced to account for the roughness property

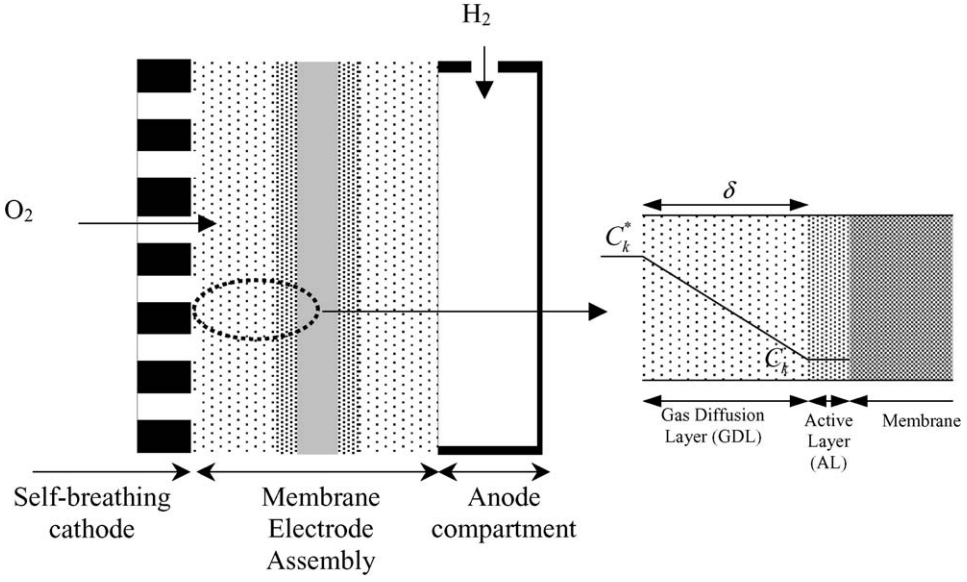

Fig. 1. Simplified diagram of an electrode of PEMFC.

of the porous active layer. It means that the catalyst particles are distributed in all the volume of the active layer.

From Eq. (2), it is then useful to express each electrode potential in terms of current density:

$$E_k = E_{\mathrm{th}_k} + \frac{b_k}{2.3} \ln \left[\frac{j_k}{\gamma_k \cdot j_{0k} \left(1 - \frac{j_k}{j_{lk}}\right)} \right] \tag{5}$$

where E_{th_k} is the thermodynamic potential of the electrode. Calculating the overpotentials of cathode and anode and fixing the values of the electrochemical parameters, the polarization curve, i.e., U_{cell} as a function of current density j, can then be plotted. Thus, by subtracting the ohmic drop ($R_{\mathrm{m}} \cdot j$) and the absolute values of overpotentials of cathode and anode from the reversible thermodynamic potential of the fuel cell (1.23 V), the polarization curve is given by

$$U_{\mathrm{cell}} = 1.23 - |\eta_{\mathrm{a}}| - |\eta_{\mathrm{c}}| - R_{\mathrm{m}} \cdot j \tag{6}$$

2.3. Modeling in dynamic regime

For the dynamic and small signal mode, the same assumptions have been conceived as those supposed in the stationary regime.

2.3.1. Analytic electrical model of fuel cell

When there is no mass transport limitation, the redox reaction is simply represented by an equivalent electrical circuit of parallel RC cells. However, when there are considerable variations of the interfacial concentrations on electrodes, the redox reaction is represented by an equivalent circuit of parallel $Z_{\mathrm{f}}C$ [15]. The faradic impedance Z_{f} is composed of two impedances in series: a charge transfer resistance R_{t} and an impedance of diffusion of the reduced species on cathode side or oxidized species on anode side. This impedance of diffusion is called Warburg impedance and is represented by Z_{W} [15,17].

The impedance of an electrode then corresponds to the parallel combination of the faradic impedance Z_{f} and the double layer capacitance (C_{dl}) to account for the dynamics of the changing concentration in the gas backing layer and the charge stored in the interfacial capacitance. The expression of the electrode impedance is thus given by:

$$Z(\omega) = \frac{Z_{\mathrm{f}}(\omega)}{1 + i\omega C_{\mathrm{dl}} Z_{\mathrm{f}}(\omega)} \tag{7}$$

Finally, the total impedance of the fuel cell is composed of two impedances, one impedance for each electrode (anode and cathode), in series with the internal resistance R_{m} linked to the membrane (Fig. 2). The total impedance Z_{Total} of the fuel cell is then given by:

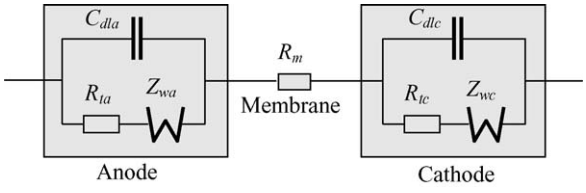

Fig. 2. Complete equivalent circuit of the fuel cell.

$$Z_{\mathrm{Total}}(\omega) = Z_{\mathrm{a}}(\omega) + R_{\mathrm{m}} + Z_{\mathrm{c}}(\omega) \tag{8}$$

Around a stationary operating point, we obtain the charge transfer resistance R_{tk} by differentiating the Eq. (3) with respect to the over potential (η):

$$R_{\mathrm{tk}} = \frac{1}{\partial j_k / \partial \eta_k} = \frac{1}{\gamma_k j_{0k} \frac{2.3}{b_k} \exp\left(\frac{2.3|\eta_k|}{b_k}\right)\left(1 - \frac{j}{j_{lk}}\right)} \tag{9}$$

while the analytical impedance of mass diffusion (i.e. Warburg impedance) is expressed as [15,17]:

$$Z_{\mathrm{W}k}(s) = \frac{\partial j_k / \partial C_k}{\partial j_k / \partial \eta_k} \frac{\delta}{n_{\mathrm{e}} F D_k^{\mathrm{eff}}} \frac{\tanh(\sqrt{s\tau_k})}{\sqrt{s\tau_k}} \tag{10}$$

where $s = I,\omega$ is the Laplace operator, and $\tau_k = \delta^2 / D_k^{\mathrm{eff}}$, the time constant of diffusion.

Here, Eq. (10) can be simplified introducing the non-linear term $A_k(j)$ which depends on the current

$$Z_{\mathrm{W}k}(s) = A_k(j) \frac{\tanh(\sqrt{s\tau_k})}{\sqrt{s\tau_k}} \quad \text{where} \quad A_k(j) = \frac{1}{\frac{2.3}{b_k}\left(1 - \frac{j}{j_{lk}}\right) C_k^*} \frac{\delta}{n_{\mathrm{e}} F D_k^{\mathrm{eff}}} \tag{11}$$

The effective double layer capacitance $C_{\mathrm{dl}}^{\mathrm{eff}}$ is defined as $C_{\mathrm{dl}}^{\mathrm{eff}} = \gamma \cdot C_{\mathrm{dl}}$, where γ represents the roughness factor whose value is of the order of 100.

2.3.2. Distributed parameter modeling approach

The presence of the tangent hyperbolic function in the analytical expression of the Warburg impedance does not enable us to draw an equivalent electrical circuit which is directly usable to model the transient response of the fuel cell in any operating mode.

The classical approach of modeling Warburg impedance consists in the decomposition of the tangent hyperbolic function in the form of a series (theoretically infinite) and in the identification of these serial terms of the RC cells parameters. The principal drawback of this approach is that it required a truncation if the infinite series. The order of truncation is chosen according to a certain tolerable error. Currently, it is the major problem related to the modeling of systems with distributed parameters of infinite order.

The decomposition of the function tanh in the form of a series (series of Foster) is given by [16] (Fig. 3):

$$\tanh(x) = 2x \sum_{n=1}^{\infty} \frac{1}{x^2 + \left[\frac{\pi(2n-1)}{2}\right]^2}$$

The Warburg impedance (Eq. (11)) then becomes:

$$Z_{\mathrm{W}k}(s) = 2A_k(j) \sum_{n=1}^{\infty} \frac{1}{s\tau_k + \left[\frac{\pi(2n-1)}{2}\right]^2} \tag{12}$$

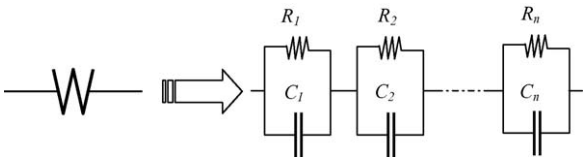

Fig. 3. Foster series equivalent of Warburg impedance.

We can then model this Warburg impedance by infinite number of parallel RC cells connected in series:

The expression of resistance R_n and capacitance C_n for each cell n is given by

$$R_n = \frac{2A(j)}{\left[\frac{\pi(2n-1)}{2}\right]^2} \quad \text{and} \quad C_n = \frac{\tau\left[\frac{\pi(2n-1)}{2}\right]^2}{2A(j)}$$

It should be noted that these parameters depend on the current density j.

2.3.3. Non-integer order modeling

Non-integer derivatives are introduced in Eq. (11) using another approximation, i.e., the second-order Taylor's expansion of the tanh function [16]:

$$\frac{\tanh(\sqrt{s\tau})}{\sqrt{s\tau}} = \frac{\sinh(\sqrt{s\tau})}{\cosh(\sqrt{s\tau})}\frac{1}{\sqrt{s\tau}} \approx \frac{\sqrt{s\tau}}{1+\frac{s\tau}{2}}\frac{1}{\sqrt{s\tau}} \approx \frac{1}{\sqrt{1+s\tau}} \tag{13}$$

This limited expansion however remains valid at high frequencies; indeed, using the approximation of tanh function for high frequencies:

$$\frac{\tanh(\sqrt{s\tau})}{\sqrt{s\tau}} = \frac{\sinh(\sqrt{s\tau})}{\cosh(\sqrt{s\tau})}\frac{1}{\sqrt{s\tau}} \underset{\infty}{\approx} \frac{e^{\sqrt{s\tau}}}{e^{\sqrt{s\tau}}}\frac{1}{\sqrt{s\tau}} \underset{\infty}{\approx} \frac{1}{\sqrt{s\tau}} \underset{\infty}{\approx} \frac{1}{\sqrt{1+s\tau}} \tag{14}$$

By using the approximation (13) we can simplify the analytical expression of the Warburg impedance given by the Eq. (11), as follows:

$$Z_{Wk}(s) = \frac{A_k(j)}{\sqrt{1+s\tau_k}} \tag{15}$$

The half-order fractional model of the Faradic impedance is then given by

$$Z_{fk}(s) = R_{tk} + Z_{Wk}(s) = R_{tk} + \frac{A_k(j)}{\sqrt{1+s\tau_k}} \tag{16}$$

The total impedance of the electrode is then given by

$$Z_{\text{electrode}}(s) = \frac{1}{\frac{1}{Z_{fk}(s)} + sC_{\text{dl}}^{\text{eff}}} \tag{17}$$

Finally, the total impedance of the fuel cell is as usually given by the relation (8).

2.4. Comparison of different models

In Fig. 4, the various models of Warburg impedance, presented in Section 2.3, are compared in frequency domain, i.e.,

- Analytical Warburg impedance given by Eq. (11).
- Classical model given by Eq. (12) using 20 RC-cells in series.
- Half-order fractional model given by Eq. (14).

These curves have been simulated for $A(j) = 1.0\,\Omega\,\text{rad}^{1/2}$ and $\tau = \delta^2/D = 1$ s. Thus, it can be noted that the difference between the fractional Warburg impedance and the analytical Warburg impedance is very small over a wide range of frequencies. This small difference that exists between the two models can be related to the second-order expansion of the tangent hyperbolic function. This limited expansion however remains valid at high frequencies.

It is also worth mentioning that the fractional Warburg impedance represents resistive behavior at low frequency, which is easily observable by a horizontal line (Fig. 4a) and is characterized by a zero phase (Fig. 4b). Moreover, asymptotically, the Bode plot of fractional model is a straight line having a slope of −10 dB per decade; while its phase is constant and equal to −45°. The asymptotic behavior of Warburg impedance is then totally taken into account by the fractional model contrary to the classical one, which behaves like a capacitance for high frequencies. The number of parameters describing each model can also be highlighted: 2 for fractional model and 40 for the classical R-C one!

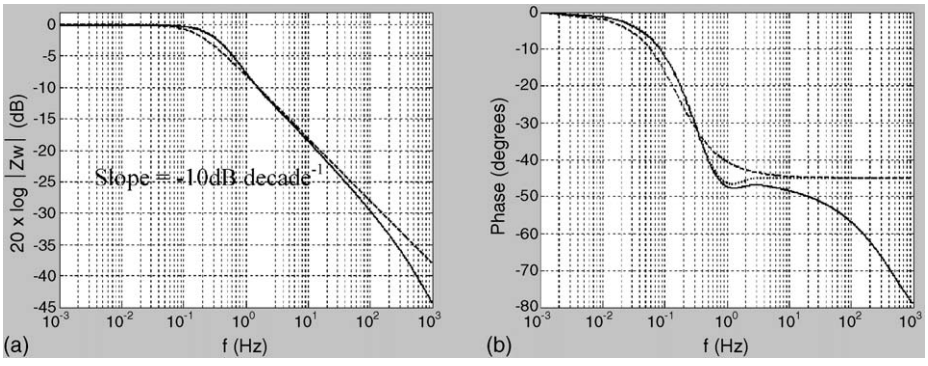

Fig. 4. Comparison of Warburg impedance, analytical expression (····), classical model using 20 RC cells (—), fractional model (- - -). (a) Variation of gain of impedance. (b) Variation of phase.

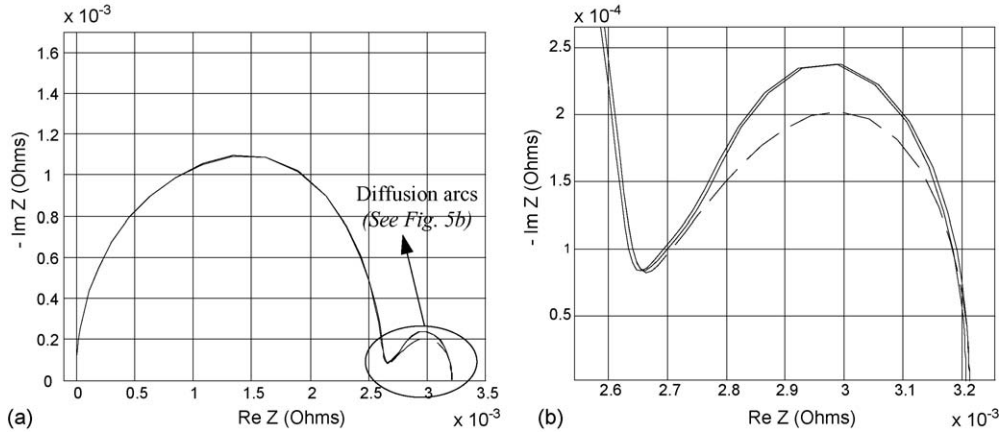

Fig. 5. Comparison between different models of impedance (in Ohms) for $j = 1.2\ \mathrm{A\ cm^{-2}}$, analytical expression (—), classical model using 20 RC cells (····), Fractional model (- - -). (a) Total impedance of the PEMFC. (b) Zoom on the diffusion arcs.

Similarly, the total impedance of the fuel cell, using the two different models of Warburg impedance can be compared (Fig. 5).Therefore, Fig. 5 shows that the classical model with (R-C) cells seems to be more precise than the fractional model, particularly in the range of frequencies where the diffusion phenomenon appears, i.e., 0.1 and 100 Hz (Figs. 4 and 5). However, the overall shape of the fractional model is in a good agreement with the shape obtained from the analytical impedance. Although there exists a mean error of 0.18% compared to the analytical expression on a given frequency range, this error is negligible for the reduced number of parameters of this model. However, it is important to note that this error depends on the current density and that its value increases with current density but remains lower than 0.5%.

In spite of this inconvenience, the important point to be noted is that the number of parameters of the fractional model is reduced. Indeed, the classical (R-C) model has $2 \times N$ parameters for N cells (R-C) in series, while the fractional model is characterized only by 2 parameters. It is a consequence of the intrinsic compactness of the fractional systems. This property, which leads to system order reduction, allows decreasing the simulation times of PEMFC system.

3. Validation of non-integer order model

3.1. Experimentation

Impedance measurements were carried out on a commercially available air-breathing PEM fuel cell provided by PAX-ITECH. It contained a Nafion®-115 membrane. The platinum loading on the electrodes was $0.3\ \mathrm{mg\ cm^{-2}}$. The electrode surface area was $25\ \mathrm{cm^2}$ and the diffusion layer thickness of 200 μm. The experimental results were obtained at ambient temperature (30 °C) while the cell functioned with air at cathode and hydrogen at anode. The test bench consisted of a Solartron 1250 frequency response analyzer coupled to a Solartron 1286 electrochemical interface. EIS experiments were performed under galvanostatic mode with modulating AC current amplitude of 100mA and range of the frequency lies between 100 mHz and 65 kHz with 10 points per decade.

In order to study the fuel cell, impedance measurements were made at open circuit and at various points along the polarization curve by changing the load resistance in order to vary the output current of the cell [18,19]. All the impedance spectra shown in Fig. 6 are modified with respect to the corresponding load resistance.

From the impedance diagrams of fuel cell, it is possible to determine a set of parameters. The high frequency intercept at real axis corresponds to the value of the internal resistance R_i of which a fraction corresponds to the membrane resistance, R_m; here, it varies approximately between 0.23 and 0.32 Ω. Moreover, the low frequency limit is the polarization resistance R_P, which is defined as the derivative (i.e. the slope) of the polarization curve of the cell. In Fig. 6, from diagram *a* to diagram *k*, R_P varies approximately from 3 to 0.4 Ω, and then it becomes almost constant at 0.4 Ω.

In Fig. 6b and c, the diagrams of impedance are composed of only single arc. This shows that at low current densities, the impedance of fuel cell is dominated by the phenomenon of charge transfer. At low frequencies (i.e. for the frequencies lower than 0.5 Hz) the diagrams of impedance do not have a particular form, and we cannot give their physical significance. In this study, we will ignore these points corresponding to the frequencies lower than 0.5 Hz. Moreover, it is well known that for high current densities, the diagrams of impedance are classically made of two arcs: the first one, the high frequency arc, is an arc of charge transfer; while the second one is an arc related to mass transport phenomenon in the diffusion layer (mainly due to the diffusion of oxygen at cathode). Moreover, it can be stated from literature [20] that the arc related to charge transfer (i.e. the high frequency arc) decreases, whereas the arc related to mass diffusion (i.e. the low frequency arc) increases, with the current density. However, in our measurements, these two arcs cannot be observed separately. This can be explained on the one hand by the fact that the output current of the cell is not sufficiently high and on the other hand by a high value of the double layer

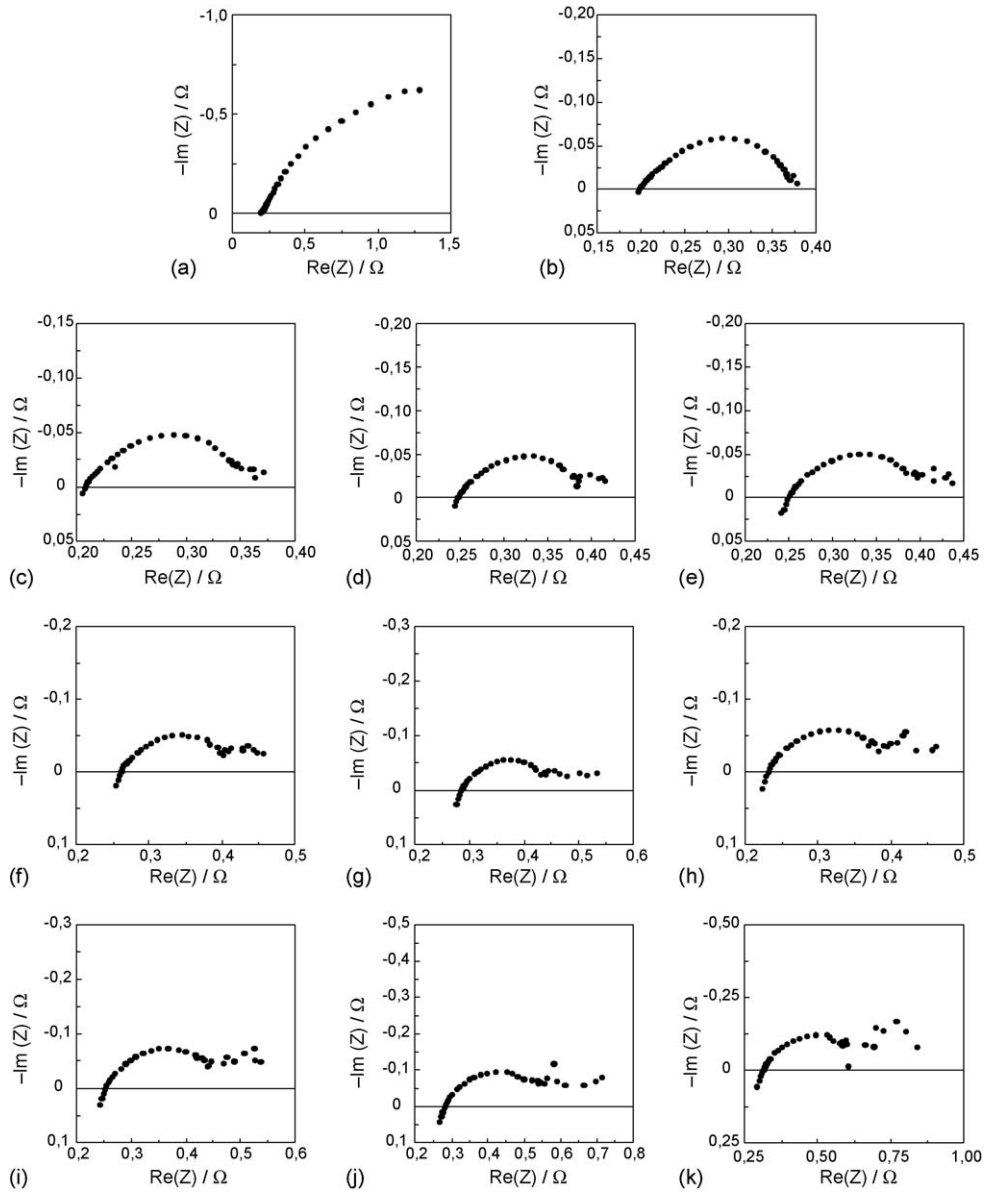

Fig. 6. Impedance diagrams of the fuel cell measured along the polarization curve. (a) Open circuit. (b) $I = 0.564$ A and $V = 0.584$ V. (c) $I = 0.906$ A and $V = 0.480$ V. (d) $I = 1.116$ A and $V = 0.411$ V. (e) $I = 1.28$ A and $V = 0.357$ V. (f) $I = 1.38$ A and $V = 0.315$ V. (g) $I = 1.512$ A and $V = 0.271$ V. (h) $I = 1.687$ A and $V = 0.244$ V. (i) $I = 1.752$ A and $V = 0.237$ V. (j) $I = 1.80$ A and $V = 0.233$ V. (k) $I = 1.84$ A and $V = 0.220$ V.

capacitance, which is hiding the two different phenomena into one arc.

3.2. Identification of model parameters

The non-linear least square fitting algorithm of MATLAB® was used to identify the relevant parameters of the fractional model of PEMFC developed in Section 2.3. The principle of this algorithm is to minimize the square of a nonlinear function while finding the best values of the unknown variables (i.e. model parameters) starting from their given initial values.

It should be noted that the impedance points measured at low frequencies, whose physical significance is not clear, and the points of impedance having a positive imaginary part (due to wiring inductance) are not taken into account for this identification process. As shown in Section 2.3, the parameters of the fractional model, which are to be identified, are R_{tk}, A_k, τ, R_m and $\gamma \cdot C_{dl}$. The effective double layer capacitance, $\gamma \cdot C_{dl}$ is determined by an algorithm of identification and then this value is used to do "fitting" for the other parameters of the model with experimental results. The value of the time constant τ is calculated from the frequency corresponding to the peak of the diffusion arc. As far as internal resistance R_i is concerned, it corresponds to the distance between the origin and the intersection of the impedance spectrum with the real axis.

The remaining parameters (R_{tk} and A_k) are identified by using non-linear least square algorithm. Table 1 shows the values of the model parameters identified for four impedance spectra corresponding to current densities ranging between 0.068 and

Table 1
Values of model parameters identified for different current densities

Parameters	$j = 0.068\ \mathrm{A\,cm^{-2}}$	$j = 0.070\ \mathrm{A\,cm^{-2}}$	$j = 0.072\ \mathrm{A\,cm^{-2}}$	$j = 0.074\ \mathrm{A\,cm^{-2}}$	Units
R_{ta}	6.67×10^{-9}	3.48×10^{-9}	2.48×10^{-9}	5.53×10^{-10}	Ω
R_{tc}	1.80×10^{-5}	1.28×10^{-5}	1.10×10^{-5}	7.0×10^{-6}	Ω
A_a	3.56×10^{-10}	1.23×10^{-8}	2.0×10^{-8}	2.62×10^{-8}	$\Omega\,\mathrm{rad}^{1/2}$
A_c	3.0×10^{-5}	4.6×10^{-5}	6.37×10^{-5}	8.4×10^{-5}	$\Omega\,\mathrm{rad}^{1/2}$
R_i	0.236	0.254	0.283	0.313	Ω
$\gamma \cdot C_{dl}$	152	115	115	115	F
τ	0.0404	0.0404	0.0404	0.0404	s
Mean error	1.41	2.56	5.50	8.22	%

$0.074\ \mathrm{A\,cm^{-2}}$, and the mean error corresponding to each set of parameters.

As expected, the four parameters, R_{ta}, R_{tc}, A_a and A_c, turn out to be more sensitive to the current density than the other ones (τ, R_i and $\gamma \cdot C_{dl}$). The evolution of the model parameters with current densities shows that the higher the output current is, more the fuel cell is limited by the diffusion phenomenon of the gases (increase in A_k); on the other hand, the charge-transfer resistance, R_{tk}, decreases with the current density. Moreover, it is clearly shown that the limitation by the diffusion phenomenon at cathode is more significant than that at the anode (i.e. $A_c > A_a$).

3.3. Validation of model parameters

The identification of the impedance spectra obtained by electrochemical impedance spectroscopy (EIS) provided a set of model parameters whose relevance must be checked. A convenient way to do this consists in comparing experimental and simulated Nyquist plots of the fuel cell at a given current density using the parameters identified in Section 3.2. Fig. 7 displays the Nyquist plots versus its fractional model fitted for the current densities of 0.068, 0.070, 0.072 and $0.074\ \mathrm{A\,cm^{-2}}$ respectively. Then, it can be observed that the results of modeling are in good agreement with the measurements.

4. Dynamic response

In previous sections, we showed that the insertion of a half-order Warburg impedance in the equivalent circuit model of the fuel cell made it possible to have a reliable and compact frequential model. The fractional approach is then at first place a frequential approach. Before concluding this paper, it seemed

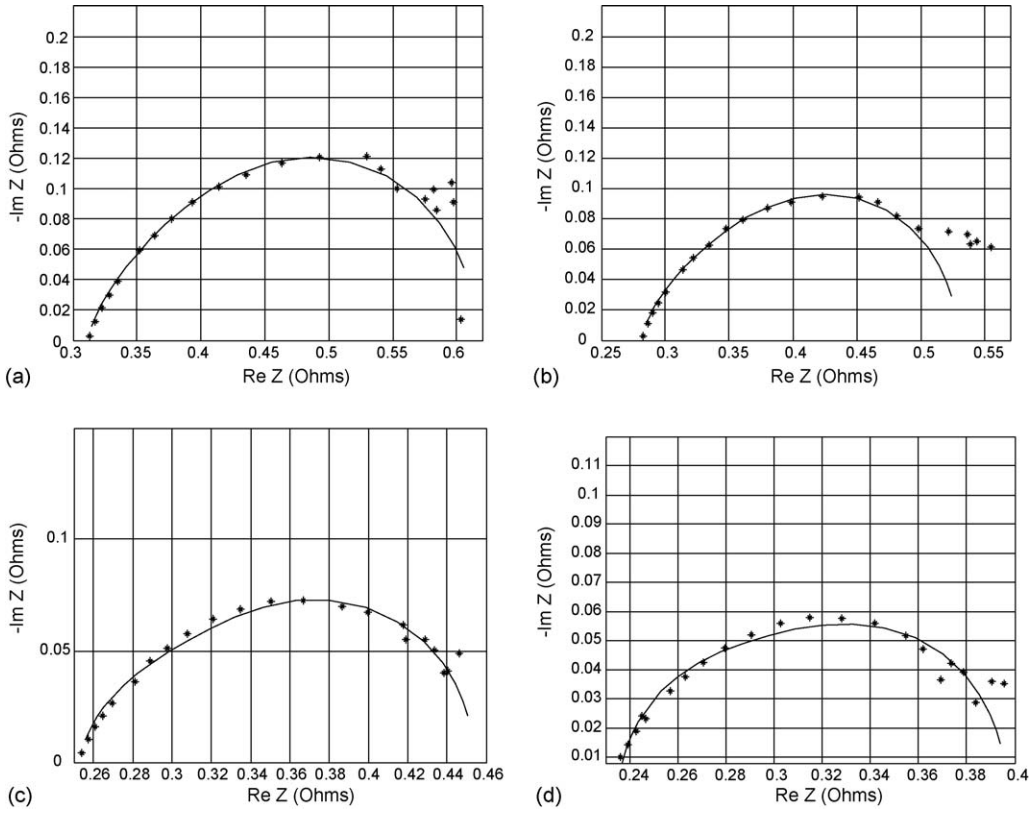

Fig. 7. Impedance spectra of the fuel cell versus its fractional model fitted for, measured (*), simulated (—) (a) $j = 0.068\ \mathrm{A\,cm^{-2}}$, (b) $j = 0.07\ \mathrm{A\,cm^{-2}}$, (c) $j = 0.072\ \mathrm{A\,cm^{-2}}$, (d) $j = 0.074\ \mathrm{A\,cm^{-2}}$.

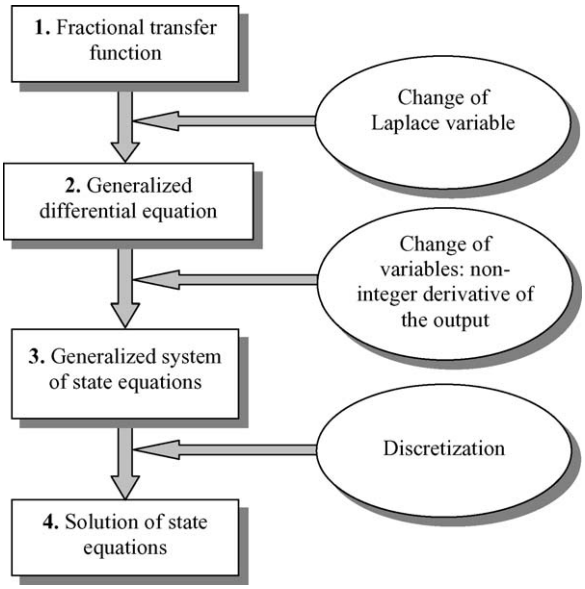

Fig. 8. Steps for calculating the time domain response of a system containing non-integer derivatives.

however essential to us to transform this frequential model into time domain, which is an obligatory step for the study of the dynamic behavior of the fuel cell.

The principal steps of the generalized algorithm for calculating the time response of a fractional system containing non-integer derivatives are summarized in Fig. 8 [16].

Each step of this algorithm, which involves extensive calculations, is described in Appendix A. This algorithm has been applied to determine the time response of the air-breathing

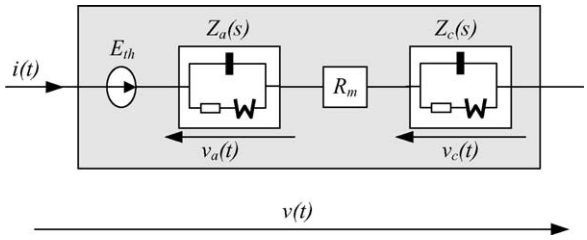

Fig. 9. Simplified schematic of a PEMFC.

PEMFC studied in Section 3. In order to find the transfer function of the fuel cell, the load current $i(t)$ is taken as input of the model, and the voltage across its terminals $v(t)$, as its output. The equivalent circuit of the fuel cell is shown in Fig. 9. The reversible thermodynamic potential E_{th} (=1.23 V) of the fuel cell is represented by a DC voltage source.

The fractional transfer function of an electrode is given by

$$Z_k(s) = \frac{V_k(s)}{I(s)} = \frac{\frac{1}{sC_{\text{dl}}^{\text{eff}}}\left[R_{\text{t}k}(j) + Z_{\text{W}k}^{1/2}(s)\right]}{\frac{1}{sC_{\text{dl}}^{\text{eff}}} + R_{\text{t}k}(j) + Z_{\text{W}k}^{1/2}(s)}$$

where

$$Z_{\text{W}k}^{1/2}(s) = \frac{A_k(j)}{\sqrt{1+\frac{s}{\omega_{0k}}}} = \frac{A_k(j)\cdot\sqrt{\omega_{0k}}}{\sqrt{s+\omega_{0k}}} \tag{18}$$

where $V_k(s)$ represents the Laplace transform of $v_k(t)$, and $\omega_{0k} = 1/\tau_{0k}$ the angular cut-off frequency. After the application of the algorithm described above, the output voltage $v(t)$ of the

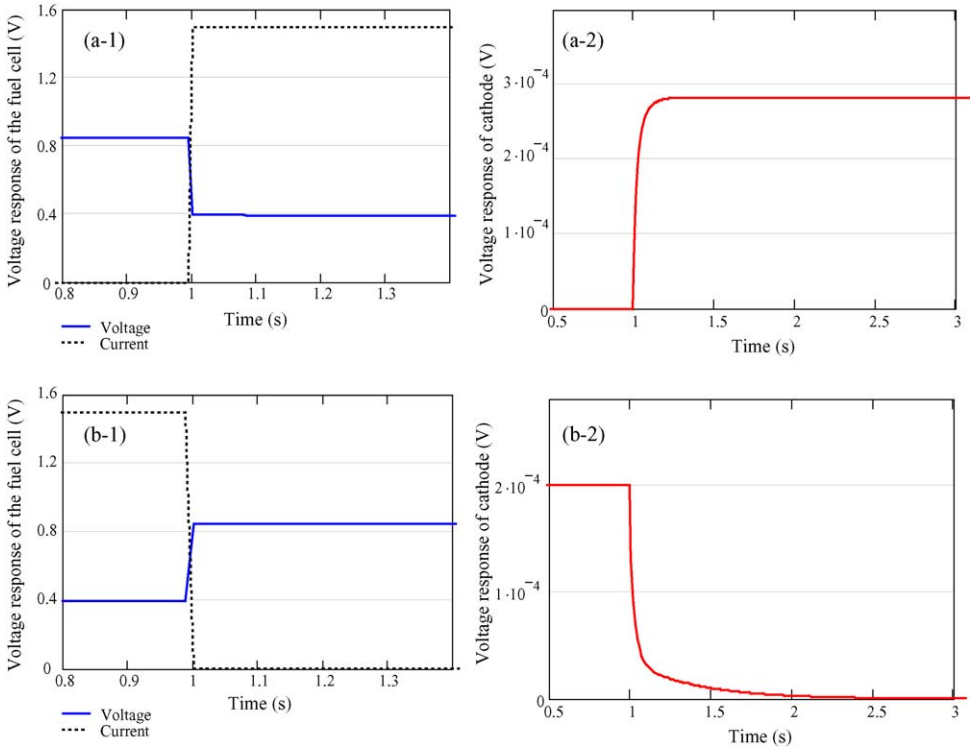

Fig. 10. Simulated voltage responses of the fuel cell and the cathode for: (a) rising step input; (b) falling step input.

Table 2
Values of model parameters obtained for $j = 0.06\ \mathrm{A\ cm^{-2}}$

Parameters	Values	Units
R_{ta}	1.94×10^{-8}	Ω
R_{tc}	3.27×10^{-5}	Ω
A_a	~ 0	$\Omega\ \mathrm{rad}^{1/2}$
A_c	4.858×10^{-6}	$\Omega\ \mathrm{rad}^{1/2}$
R_m	0.3	Ω
$\gamma \cdot C_{dl}$	152	F
τ	0.0404	s

fuel cell is then given by the following equation:

$$v(t) = E_{th} - £^{-1}\{Z_a(s)I(s)\} - £^{-1}\{Z_c(s)I(s)\} - R_m i(t) \quad (19)$$

where $I(s)$ represents the Laplace transform of the input current $i(t)$.

In order to find the voltage response of the fractional model, two types of input signals $i(t)$ were applied; a rising step signal of amplitude 1.5A (Fig. 10a-1), and another falling step signal, of the same amplitude (Fig. 10b-1). The final results of the simulation of the voltage response of the fuel cell (Fig. 10, a-1 and b-1) and of cathode (Fig. 10, a-2 and b-2) are shown on Fig. 10.

For the simulation of Fig. 10, the values of the parameters identified by EIS (in Section 3) were linearly extrapolated in order to obtain the parameters corresponding to 1.5 A (i.e. $j = 0.06\ \mathrm{A\ cm^{-2}}$). These values are given in Table 2. Note that the transient response is in good agreement with the time response of the gas transport [12].

5. Experimental validation of time response

In this section, the dynamic response, derived from the fractional model of PEMFC in Section 4, has been experimentally validated.

In order to experimentally measure the dynamic response of a commercial air-breathing PEMFC on the test bench, a periodic square wave signal of the current of amplitude 1.5 A and frequency 0.1 Hz was imposed at the fuel cell terminals by an electronic load. The corresponding variations in the cell voltage were then recorded; the results are shown in Fig. 11. These measurements were made at the ambient temperature (30 °C).

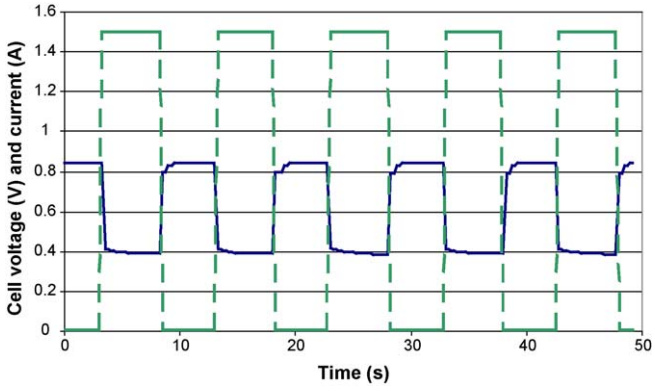

Fig. 11. Measured dynamic response of the air-breathing PEMFC, cell voltage (—), cell current (- - -).

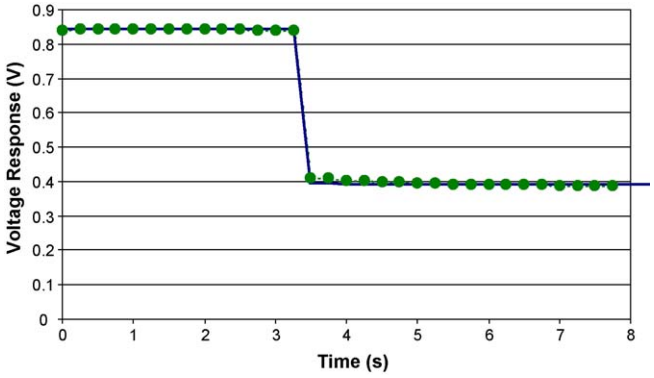

Fig. 12. Comparison of measured and simulated dynamic responses of the PEMFC, simulated (—), measured (- - -).

The results of simulation (Fig. 10) and experimental measurement (Fig. 11) are compared for a period in Fig. 12. It is observable that the modeling results are in good agreement with the measurements. The mean error over this period is equal to 0.64%, and the maximum error is about 4.13%.

6. Conclusions

A fine and compact frequential model of a PEMFC taking account of the diffusion and charge-transfer phenomena was presented in this paper. This new modeling technique distinguishes completely from the traditional approaches since it uses non-integer derivation. In particular it makes possible to reach a model of the fuel cell, reliable on a wide range of frequencies with a limited number of parameters. Moreover, each parameter of the model has a physical significance.

The technique of electrochemical impedance spectroscopy was demonstrated as a powerful tool in order to validate this model. Lastly, a general algorithm for calculating the time response of fractional systems was used for the simulation of the transient state of the fuel cell. In order to validate the simulated dynamic behavior of the fuel cell, a commercial air-breathing PEMFC was subjected to rapid variations in the load current and the output voltage was recorded. The results of simulation were found in good agreement with experimental results.

However, a further study is necessary for the development of a more specific algorithm for the simulation of the transient response. The major work needed in future consists in defining more systematic methods for identification of the parameters and their validation particularly in the time domain. Moreover, it would also be interesting to study in detail the influence of the working conditions and geometrical parameters of the fuel cell (i.e. geometry of electrodes, the thickness and the type of membrane etc.) on the model parameters.

Appendix A. Calculation of time response of the fuel cell

Step 1: Definition of the transfer function

We can describe a system in the form of a transfer function between an output O and an input I, as: $F(s) = \frac{O(s)}{I(s)}$ where O

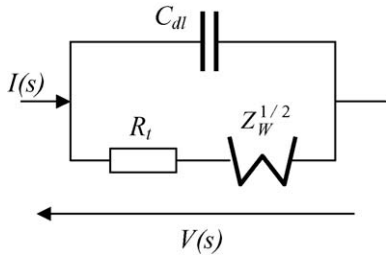

Fig. A1. Schematic of an electrode.

and I indicate the Laplace transforms of the functions o and i, respectively. The objective is of course to determine the output $o(t)$ for a given input $i(t)$.

Generally, the function $F(s)$ can be written in the form of a quotient of two polynomials $A(s)$ and $B(s)$, each containing the integer derivatives of s and one or more implicit systems of fractional nature all of the same angular cut-off frequency $\omega_0 = 1/\tau_0$.

First of all, we can write an operational relation between the current $I(s)$ and the voltage $V(s)$ for a single electrode (Fig. A1):

$$\frac{V(s)}{I(s)} = \frac{\frac{1}{sC_{\mathrm{dl}}}[R_{\mathrm{t}}(j) + Z_{\mathrm{W}}^{1/2}(s)]}{\frac{1}{sC_{\mathrm{dl}}} + R_{\mathrm{t}}(j) + Z_{\mathrm{W}}^{1/2}(s)} \tag{A.1}$$

where

$$Z_{\mathrm{W}}^{1/2}(s) = \frac{A(j)}{\sqrt{1 + \frac{s}{\omega_0}}} = \frac{A(j) \cdot \sqrt{\omega_0}}{\sqrt{s + \omega_0}}$$

where j represents the current density. In this case, $A(s)$ and $B(s)$ are defined by

$$A(s) = R_{\mathrm{t}}(j) + Z_{\mathrm{W}}^{1/2}(s)$$

$$B(s) = 1 + sC_{\mathrm{dl}} \cdot R_{\mathrm{t}}(j) + sC_{\mathrm{dl}} \cdot Z_{\mathrm{W}}^{1/2}(s)$$

Step 2: Change of the variable of Laplace

The second step consists of carrying out the change of the variable of Laplace, i.e., $s_1 = s + \omega_0$.

In effect, the transfer function (A.1) becomes a rational fraction of polynomials in s_1 of only integer and non-integer orders:

$$\frac{V(s_1 - \omega_0)}{I(s_1 - \omega_0)} = \frac{A(s_1 - \omega_0)}{B(s_1 - \omega_0)} = \frac{A_0 + A_{1/2}s_1^{1/2}}{B_0 + B_{1/2}s_1^{1/2} + B_1 s_1^1 + B_{3/2}s_1^{3/2}} \tag{A.2}$$

where

$$A_0 = \frac{A(j) \cdot \omega_{\mathrm{o}}^{1/2}}{C_{\mathrm{dl}}}, \qquad A_{1/2} = \frac{R_{\mathrm{t}}(j)}{C_{\mathrm{dl}}}$$

$$B_0 = -A(j) \cdot \omega_{\mathrm{o}}^{3/2}, \qquad B_{1/2} = \frac{1}{C_{\mathrm{dl}}} - \omega_{\mathrm{o}} \cdot R_{\mathrm{t}}(j)$$

$$B_1 = A(j) \cdot \omega_{\mathrm{o}}^{1/2}, \qquad B_{3/2} = R_{\mathrm{t}}(j)$$

Step 3: Generalized differential equation

The Eq. (A.2) can also be written in the form:

$$B_0 \cdot V(s_1 - \omega_0) + B_{1/2}s_1^{1/2}V(s_1 - \omega_0) + B_1 s_1^1 V(s_1 - \omega_0) + B_{3/2}s_1^{3/2}V(s_1 - \omega_0) = A_0 I(s_1 - \omega_0) + A_{1/2}s_1^{1/2}I(s_1 - \omega_0) \tag{A.3}$$

We know that [12]:

$$s_1^{\alpha} \cdot G(s_1 - \omega_0) = \pounds\,\{D^{(\alpha)}[g(t) \cdot \exp(t\omega_0)]; s_1\}$$

where G is the Laplace transform of the function g. If we apply the inverse Laplace transform to the Eq. (A.3), the following generalized differential equation is obtained:

$$B_0 v(t)\exp(t\omega_0) + B_{1/2}D^{(1/2)}[v(t)\exp(t\omega_0)] + B_1 D^{(1)}[v(t)\exp(t\omega_0)] + B_{3/2}D^{(3/2)}[v(t)\ \exp(t\omega_0)] = A_0 i(t)\exp(t\omega_0) + A_{1/2}D^{(1/2)}[i(t)\exp(t\omega_0)] \tag{A.4}$$

In order to simplify the notations, we consider next the variables $s(t)$ and $e(t)$ such that:

$$s(t) = v(t) \cdot \exp(t\omega_0), \qquad e(t) = i(t) \cdot \exp(t\omega_0)$$

By dividing each term of the Eq. (A.4) by $B_{3/2}$, we can then write

$$\frac{B_0}{B_{3/2}}s(t) + \frac{B_{1/2}}{B_{3/2}}s^{(1/2)}(t) + \frac{B_1}{B_{3/2}}s^{(1)}(t) + s^{(3/2)}(t) = E(t) \tag{A.5}$$

where

$$E(t) = \frac{A_0 e(t) + A_{1/2}\mathrm{e}^{(1/2)}(t)}{B_{3/2}}$$

Step 4: Change of variables: non-integer derivative of the output

The change of variables carried out in this step is the key of this algorithm of calculating time response. Indeed, it is the operation which will enable us to build the generalized system of state equations, and thus to solve the problem.

The system (A.6) below clarifies better this change of variable:

$$s(t) = x_1(t), \qquad s^{(1/2)}(t) = D^{(1/2)}s(t) = x_1^{(1/2)}(t) = x_2(t),$$
$$s^{(1)}(t) = D^{(1)}s(t) = x_2^{(1/2)}(t) = x_3(t),$$
$$s^{(3/2)}(t) = D^{(3/2)}s(t) = x_3^{(1/2)}(t) = x_4(t) \tag{A.6}$$

The unknown to be determined is of course x_1.

Step 5: Construction of generalized system of state equations

By using the change of variables defined by the system (A.6), the Eq. (A.5) can be written in the form:

$$x_3^{(1/2)}(t) = x_4(t) = -a_1x_1(t) - a_2x_2(t) - a_3x_3(t) + E(t) \tag{A.7}$$

with

$$a_1 = \frac{B_0}{B_{3/2}}, \qquad a_2 = \frac{B_{1/2}}{B_{3/2}} \quad \text{and} \quad a_2 = \frac{B_{1/2}}{B_{3/2}}$$

From the Eqs. (A.6) and (A.7), one can then write the generalized system of state equations between the input vector $e(t)$, the state vector $x(t) = [x_1(t), x_2(t), x_3(t)]^T$, and the output vector $s(t)$:

$$x^{(1/2)}(t) = A \cdot x(t) + B \cdot e(t), \qquad s(t) = C \cdot x(t) + D \cdot e(t)$$

where

$$A = \begin{bmatrix} 0 & 1 & 0 \\ 0 & 0 & 1 \\ -a_1 & -a_2 & -a_3 \end{bmatrix}, \qquad B = \begin{bmatrix} 0 \\ 0 \\ 1 \end{bmatrix},$$

$$C = \begin{bmatrix} 1 & 0 & 0 \end{bmatrix}, \qquad D = 0 \tag{A.8}$$

Step 6: Discretization

In order to solve the problem, we will first of all modify the form of the system of state equations; starting from the relations (A.7) and (A.8):

$$x_1^{(1/2)}(t) - x_2(t) = 0, \qquad x_2^{(1/2)}(t) - x_3(t) = 0,$$

$$x_3^{(1/2)}(t) + a_1x_1(t) + a_2x_2(t) + a_3x_3(t) = E(t) \tag{A.9}$$

Then, we compute each variable with a step size of h. The following relation gives an approximation of the non-integer derivative of a function at a sampling instant $t_m = m{\cdot}h$, [12]:

$$x_j^{(v_j)}(t_m) = \sum_{k=0}^{m} \lambda_{v_j}(k) \cdot x_j[(m-k) \cdot h] \tag{A.10}$$

where

$$\lambda_{v_j}(k) = \begin{cases} (-1)^k \dfrac{v_j(v_j-1) \times \cdots \times (v_j-k+1)}{h^{v_j}k!} & \text{for } k \geq 1 \\ \dfrac{1}{h^{v_j}} & \text{for } k = 0 \end{cases}$$

where v_j indicates the order of the derivation of the variable x_j. In the next we will consider for $k \geq 1$:

$$\omega_{v_j}(k) = (-1)^k \frac{v_j(v_j-1) \times \cdots \times (v_j-k+1)}{k!}$$

Eq. (A.10) can then be written in the form:

$$x_j^{v_j}(t_m) = \frac{1}{h^{v_j}} \cdot x_j(t_m) + \frac{1}{h^{v_j}} \cdot \sum_{k=1}^{m} \omega_{v_j}(k) \cdot x_j[(m-k) \cdot h] \tag{A.11}$$

The first term at right-hand side corresponds to what we are seeking to calculate at the instant t_m ($t_m = m{\cdot}h$), the sum $Q_j(m{\cdot}h)$ corresponds to the samples calculated at the previous instants. Applying the expression (A.11), for each state variable of the system (A.9), we obtain:

$$\begin{bmatrix} h^{-1/2} & -1 & 0 \\ 0 & h^{-1/2} & -1 \\ a_1 & a_2 & a_3 + h^{-1/2} \end{bmatrix} \cdot \begin{bmatrix} x_1(mh) \\ x_2(mh) \\ x_3(mh) \end{bmatrix} = \begin{bmatrix} -Q_1(mh) \\ -Q_2(mh) \\ -Q_3(mh) + E(mh) \end{bmatrix} \tag{A.12}$$

Step 7: Solution of the system

By inversing the matrix M defined in the relation (A.12), it is then possible to determine the value of each state variable at any instant and particularly that in which we are interested, namely x_1. By multiplying this variable by the term $\exp(-t/\tau_o)$ for every instant t, we finally obtain the variable $v(t)$. Following the same steps for the anode and cathode, and then using the equation of polarization of the fuel cell, subtracting the ohmic drop in the membrane, cell voltage can be plotted with respect to time.

$$U_{cell}(t) = 1.23 - |v_a(t)| - |v_c(t)| - R_m \cdot i(t)$$

where $v_a(t)$ and $v_c(t)$ are the output voltages of the anode and cathode respectively, determined using the above algorithm.

References

[1] D.M. Bernardi, Water-balance calculation for solid polymer electrolyte fuel cells, J. Electrochem. Soc. 137 (1990) 3344–3350.

[2] T.V. Nguyen, R.E. White, A water and heat management model for proton-exchange-membrane-fuel-cell, J. Electrochem. Soc. 140 (1993) 2178–2186.

[3] T.E. Springer, T.A. Zawodzinski, S. Gottesfeld, Polymer electrolyte fuel cell model, J. Electrochem. Soc. 138 (1991) 2334–2342.

[4] G. Murgia, L. Pisani, M. Valentini, B.D. Aguanno, Electrochemistry and mass transport in polymer electrolyte membrane fuel cells, J. Electrochem. Soc. 149 (2002) A31–A38.

[5] D.M. Bernardi, M.K. Verbrugge, A mathematical model of the solid-polymer-electrolyte fuel cell, J. Electrochem. Soc. 139 (1992) 2477–2491.

[6] T.E. Springer, M.S. Wilson, S. Gottesfeld, Modeling and experimental diagnostics in polymer electrolyte fuel cells, J. Electrochem. Soc. 140 (1993) 3513–3526.

[7] J.S. Yi, T.V. Nguyen, Multicomponent transport in porous electrode of proton exchange membrane fuel cell using interdigitated gas distributor, J. Electrochem. Soc. 146 (1999) 38–45.

[8] D. Natarajan, T.V. Nguyen, A two-dimensional, two-phase, multicomponent, transient model for the cathode proton exchange membrane fuel cell using conventional gas distributor, J. Electrochem. Soc. 148 (2001) A1324–A1335.

[9] N. Wagner, Characterisation of membrane-electrode assemblies in polymer electrolyte fuel cells using A.C. impedance spectroscopy, J. Appl. Electrochem. 32 (2002) 859–863.

[10] M. Ceraolo, C. Miuli, A. Pozio, Modelling static and dynamic behaviour of proton exchange membrane fuel cells on the basis of

the electro-chemical description, J. Power Sources 113 (2003) 131–144.
[11] S. Yerramalla, A. Davari, A. Feliachi, T. Biswas, Modeling and simulation of the dynamic behavior of a polymer electrolyte membrane fuel cell, J. Power Sources 124 (2003) 104–113.
[12] Y. Wang, C.Y. Wang, Transient analysis of polymer electrolyte fuel cells, Electrochim. Acta 50 (2005) 1307–1315.
[13] P.R. Pathapati, X. Xue, J. Tang, A new dynamic model for predicting transient phenomena in a PEM fuel cell system, Renewable Energy 30 (2005) 1–22.
[14] J. Garnier, J.-P. Diard, M.C. Péra, F. Harel, D. Candusso, D. Hissel, N. Glandut, A. De Bernardinis, J.-M. Kauffmann, G. Coquery, Dynamic PEMFC Modelling for Automotive Applications, vol. 1, IEEE Seminar, Oct.–Nov. 2003, ISBN 0-7803-7955-1.
[15] M. Bautista, Y. Bultel, P. Ozil, Polymer electrolyte membrane fuel cell modeling: dc and ac solutions, Trans IChemE, Part A 82 (A7) (2004) 907–917.
[16] D. Riu, N. Retière, M. Ivanès, Induced currents modeling by half-order systems application to hydro- and turbo-alternators, IEEE Trans. Energy Conversion 18 (1) (2003) 94–99.
[17] S. Walkiewicz, Y. Bultel, B. Le Gorrec, J.P. Diard, Modeling Impedance Diagrams of Fuel Cell, in 4th International Symposium on Electrocatalysis, Satellite meeting of the 53rd ISE meeting in Duesseeldorf, Abstract p. 71, 22–25 Septembre 2002, Como (Italy).
[18] J.P. Diard, B. Le Gorrec, C. Montella, C. Poinsignon, G. Vitter, Impedance measurements of polymer electrolyte fuel cells running on constant load, J. Power Sources 74 (1998) 244–245.
[19] J.P. Diard, N. Glandut, B. Le Gorrec, C. Montella, Impedance measurements of each cell of a 10 W PEMFC Stack Under Load, J. Electrochem. Soc. 151 (12) (2004) A2193–A2197.
[20] V.A. Paganin, C.L.F. Oliveira, E.A. Ticianelli, T.E. Springer, E.R. Gonzales, Modelistic interpretation of the impedance response of a polymer electrolyte membrane fuel cell, Electrochim. Acta 43 (1998) 3761–3766.